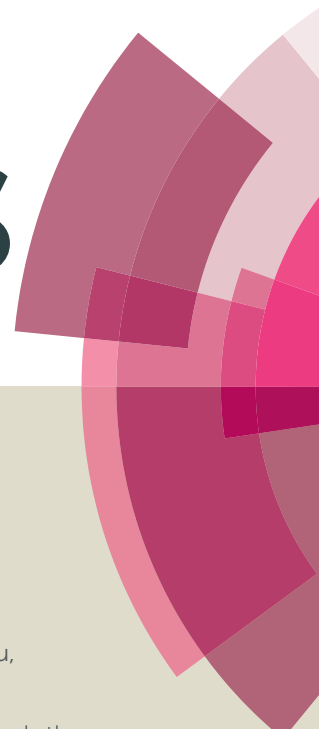


# RSC Advances



This article can be cited before page numbers have been issued, to do this please use: Z. Wang, X. Hou, J. Shen and T. Li, *RSC Adv.*, 2016, DOI: 10.1039/C6RA21442H.



This is an *Accepted Manuscript*, which has been through the Royal Society of Chemistry peer review process and has been accepted for publication.

*Accepted Manuscripts* are published online shortly after acceptance, before technical editing, formatting and proof reading. Using this free service, authors can make their results available to the community, in citable form, before we publish the edited article. This *Accepted Manuscript* will be replaced by the edited, formatted and paginated article as soon as this is available.

You can find more information about *Accepted Manuscripts* in the [Information for Authors](#).

Please note that technical editing may introduce minor changes to the text and/or graphics, which may alter content. The journal's standard [Terms & Conditions](#) and the [Ethical guidelines](#) still apply. In no event shall the Royal Society of Chemistry be held responsible for any errors or omissions in this *Accepted Manuscript* or any consequences arising from the use of any information it contains.



## Journal Name

## ARTICLE

## Supported Cobalt Oxide Nanocrystals: Morphology Control and Catalytic Performance For Styrene Oxidation

Zhen Wang,<sup>†a</sup> Xianliang Hou,<sup>†a</sup> Jingmei Shen<sup>b</sup> and Tiehu Li<sup>a\*</sup>

Received 00th January 20xx,  
Accepted 00th January 20xx

DOI: 10.1039/x0xx00000x

www.rsc.org/

Metal oxide nanoparticles with controlled size and morphology seem extremely important due to the strong correlation between these parameters and their catalytic properties. Herein supported cobalt oxide nanoparticles with controlled size and different morphologies were successfully synthesized via a facile hydrothermal synthetic route under mild conditions. The size and morphology of the products can be readily tuned by tuning process parameters such as hydrothermal time and hydrothermal temperature. As synthesized supported cobalt oxide nanoparticles, namely Co<sub>3</sub>O<sub>4</sub>-150, Co<sub>3</sub>O<sub>4</sub>-550 and Co<sub>3</sub>O<sub>4</sub>-650 respectively, were quite active for the catalytic oxidation of styrene with H<sub>2</sub>O<sub>2</sub> as a green oxidant. However, due to the size and morphology differences, these supported cobalt oxide nanoparticles exhibited different activities and selectivities. Co<sub>3</sub>O<sub>4</sub>-550 resulted in higher activity while Co<sub>3</sub>O<sub>4</sub>-650 exhibited relatively higher selectivity to epoxide. Moreover, these cobalt catalysts could be recycled, indicating this to be a promising method of fabricating supported cobalt oxide catalysts for the oxidation of olefins in large-scale processes.

### Introduction

Nanomaterials have gained extensive interests due to their applications in the field of medicine, optics, electrics, energy and catalysis.<sup>1</sup> As one of the most studied nanomaterials, cobalt oxide nanoparticles have exhibited outstanding electrochemical,<sup>2,3</sup> magnetic,<sup>4,5</sup> gas sensing<sup>6,7</sup> and catalytic<sup>8,9</sup> capabilities. On the catalytic capability of supported cobalt oxide nanoparticles are of particular interest because of their great industrial potential in the oxidation of hydrocarbons reactions, including methane combustion<sup>10</sup>, propane combustion<sup>11</sup>, cyclohexane oxidation,<sup>12</sup> CO oxidation<sup>13</sup>, etc.

In recent years, the synthesis and structural characterization of cobalt oxide nanostructures have been well established,<sup>14-18</sup> which enable us to explore the effect of particle morphology on catalytic performance, and develop rational design and synthesis of highly active catalysts. On the other hand, when materials approach nanoscale dimensions, they exhibit extremely different properties from their bulk counterparts in adsorption capacities, surface area and accessibility of the active sites, etc. Conventionally, active catalysts consist of small nanometer-sized particles, because the number of corner and edge atoms for adsorption and activation of the reactants increases with decreasing crystal domains.<sup>19-21</sup> Moreover, if metal oxide nanoparticles can be confined within a nanoporous host this may limit the size to which the metal nanoparticle can grow, as they typically sinter during preparation.

Typically nanopores serve as a confined or growing space for the loaded nanocrystals with a narrow size distribution.

Metal oxide nanoparticles with controlled size and morphology seem extremely important due to the strong correlation between these parameters and their catalytic properties. The catalytic performance for styrene oxidation is extremely sensitive to the particle size and morphologies because the surface structure and electronic properties may change considerably at different nanometer-size level. On the other hand, surface science enabled the study of the activity and selectivity of the catalysts by the characteristics at the atom-level structure of the planes that they expose.<sup>22,23</sup> It is obvious that both the activity and the selectivity of a catalyst can be tailored by tuning its morphology. Although the concept of morphology-dependent catalysis makes it possible to correlate the catalytic performance with the morphology/plane of the crystal under realistic reaction conditions, it is still challenging to synthesize catalytic nanomaterials that are enclosed by specific surface planes, hopefully the most reactive facets.

In the past we successfully designed a kind of novel compound possesses 16 carboxylic acid groups in each corner of POSS structure.<sup>24</sup> Based on this work, we became interested in applying this compound in the synthesis of supported metal oxide. Herein, we report three cobalt oxide catalysts with different size and morphologies for styrene oxidation reaction. The catalysts were successfully synthesized via a facile hydrothermal synthetic route under mild conditions. The size and morphology of the catalysts can be readily tuned by tuning process parameters such as hydrothermal time and hydrothermal temperature. It was expected that these supported cobalt oxide nanoparticles exhibited different activities and selectivities due to the size and morphology differences. Moreover, these cobalt catalysts could be recycled,

<sup>a</sup> School of Materials Science and Engineering, Northwestern Polytechnical University, Xi'an, Shaanxi 710072, P. R. China. E-mail: litiehunpu@163.com.

<sup>b</sup> Optimal CAE, R&D, 47802 West Anchor Court, Plymouth, MI 48170, US.

Electronic Supplementary Information (ESI) available: NMR, XPS, XRD, SEM, TEM, EDS, etc were included here. See DOI: 10.1039/x0xx00000x

indicating this to be a promising method of fabricating cobalt oxide catalysts for the oxidation of olefins in large-scale processes.

## Experimental

### Materials

All the solvents (anhydrous), reagents and catalysts were purchased commercially and were used without further purification. Tetrahydrofuran (anhydrous, 99.9%), Ethyl ether (anhydrous, ≥99.0%), toluene (anhydrous, ≥99.8%), benzyl alcohol (99%),  $[\text{Si}_8\text{O}_{12}]-(\text{OSiMe}_2\text{H})_8$  (95%), diethylamine (99%, Sigma-Aldrich), Pt/C (30 wt%) were purchased from Sigma-Aldrich. Allylmalonic acid (99%) was purchased from Alfa Aesar, 1,4-bis-dimethylsilylbenzene (97%) were purchased from ABCR. The Karstedt catalyst (a platinum(0) divinyl tetramethyldisiloxane complex in xylene, 2.1~2.4 wt% Pt, Gelest Inc) was used for hydrosilylation. Pt/C (30 wt%, Sigma-Aldrich) was used for the hydrogenolysis. Thin layer chromatography was performed on silica gel plates Merck 60 F254. The compounds were detected by UV lamp. Compound I and compound III were purified by silica gel column chromatography (pore size 60 Å, 70-230 mesh, Sigma-Aldrich). Experiments involving compound IV was performed in  $\text{N}_2$  glovebox or Schlenk techniques under nitrogen atmosphere. The structure of the compound I, II, III, IV were shown in Figure 1.

### Preparation of supported cobalt oxide catalysts

#### Synthesis of compound I, III, IV.

(1) Compound I. The synthesis procedure was based on the reference.<sup>24</sup> Allylmalonic acid (4.32 g, 30 mmol), benzyl alcohol (7.46 mL, 70 mmol) and anhydrous toluene (30 mL) were added to a round bottom flask. A drop of  $\text{H}_2\text{SO}_4$  (95.8%, 0.030 mL) was added under stirring. The solution was refluxed for 6 h with a Dean-Stark apparatus to remove water. The reaction was monitored with thin-layer chromatography (TLC). When the allylmalonic acid disappeared, the solution was cooled down and washed by saturated sodium bicarbonate solution, sodium chloride solution and distilled water. The desired compound I, was purified by column chromatography (eluent: hexane/ethyl acetate = 9/1 by volume). Yield: 6.39 g (95%).  $^1\text{H}$  NMR characterization is shown in Figure S1.  $^1\text{H}$  NMR ( $\text{CDCl}_3$ , 400 MHz):  $\delta$  2.67 (t, 2H, J = 7); 3.54 (t, 1H, J = 7); 5.02

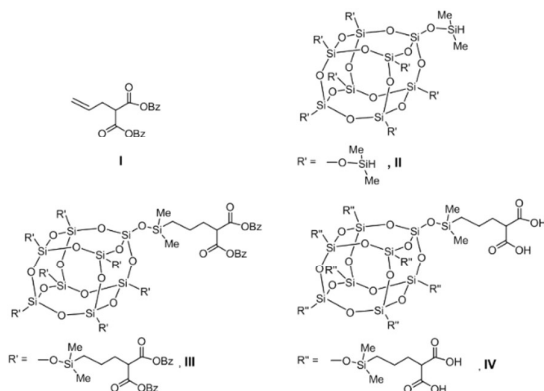
Fig. 1 The structure of compound I, II, III, IV.

(d, 1H, J = 10); 5.07 (d, 1H, J = 17); 5.13 (m, 4H); 5.76 (m, 1H); 7.19 – 7.37 (m, 10H).  $^{13}\text{C}$  NMR ( $\text{CDCl}_3$ , 100 MHz):  $\delta$  32.93; 51.77; 67.33; 117.90; 128.32; 128.46; 128.66; 133.91; 135.42; 168.73.

(2) Compound III. Compound I (2.60 g, 8.77 mmol), commercial compound II (0.893 g, 0.877 mmol), and anhydrous THF (40 mL) was loaded in a flamed dried schlenk flask. The solution was heated to 40 °C. Karstedt's catalyst (platinum divinyltetramethyldisiloxane [Pt(dvs)], 0.1 mL) was added to the solution to catalyze the hydrosilylation reaction. The reaction was monitored by  $^1\text{H}$  NMR for the disappearance of the Si-H signal. The solution was stirred for 8 h at 40 °C to reach completion. The product was purified by column chromatography. Unreacted compound I was first removed using hexane/ethyl acetate = 4/1 by volume. After that the eluent was then changed to hexane/ethyl acetate = 3/1 by volume to purify III. Yield: 2.65 g (90%). The product was characterized by  $^1\text{H}$ ,  $^{13}\text{C}$ , and  $^{29}\text{Si}$  NMR spectroscopy which were shown in Figure S2.  $^1\text{H}$  NMR ( $\text{CDCl}_3$ , 400 MHz):  $\delta$  0.043 (s, 48H); 0.56 (t, 16H, J = 8); 1.27 (m, 16H); 1.91 (q, 16H, J = 7); 3.42 (t, 8H, J = 8); 5.18 (m, 32H); 7.14 – 7.37 (m, 80H).  $^{13}\text{C}$  NMR ( $\text{CDCl}_3$ , 100 MHz):  $\delta$  -0.095; 17.55; 21.13; 32.50; 51.95; 67.26; 128.47; 128.63; 128.83; 135.81; 169.41.  $^{29}\text{Si}$  NMR ( $\text{CDCl}_3$ , 79 MHz):  $\delta$  -112.6; 8.61.

(3) Compound IV. Compound III (2.58 g) and Pd/C catalyst (30 wt%, 10 mg) were added to a flame dried schlenk flask preloaded with 50 mL, a mixed solvent MeOH/THF (1/9 by volume) under  $\text{N}_2$  atmosphere.  $\text{H}_2$  gas was then bubbled into the solution for 12 h under stirring at ambient temperature. The mixture was then filtered through a PTFE membrane syringe filter (dia. 0.45  $\mu\text{m}$ ) to remove the catalyst. The volatiles of the resulting clear filtrate were evaporated under vacuum to yield a colorless oil. The oil was further evacuated under high vacuum for overnight to afford a white solid. Yield: 1.55g (97%). The product was confirmed by  $^1\text{H}$ ,  $^{13}\text{C}$ , and  $^{29}\text{Si}$  NMR spectroscopy which were shown in Figure S3.  $^1\text{H}$  NMR ( $\text{DMSO}-d_6$ , 400 MHz):  $\delta$  0.11 (s, 48H); 0.59 (t, 16H, J = 8); 1.31 (m, 16H); 1.72 (q, 16H, J = 8); 3.22 (t, 8H, J = 8); 12.6 (s, 16H).  $^{13}\text{C}$  NMR ( $\text{THF}-d_8$ , 100 MHz):  $\delta$  0.50; 18.71; 22.41; 33.83; 52.42; 171.72.  $^{29}\text{Si}$  NMR ( $\text{THF}-d_8$ , 79 MHz):  $\delta$  -103.31; 18.30.

**Synthesis of supported cobalt nanospheres.** Compound IV (100 mmoles) was added to a schlenk flask with 4 or 8 equivalents of  $\text{Co}_2(\text{CO})_8$  in a mixture of toluene and THF solution (50 mL, 20:1 volume ratio). The reactions were allowed to stir for 24h at room temperature under  $\text{N}_2$  atmosphere. Then the precipitate was collected by filtering the mixture with diethyl ether in  $\text{N}_2$  glovebox. Concentration of the filtrate solution afforded pink precipitate as the major products with about 90% yield (based on the amount of compound IV added). The amount of cobalt precursor did not affect the yield. The pink precipitate is the as-synthesized supported cobalt nanospheres. There are several reasons that we chose POSS supported cobalt oxide as a precursor of catalyst. Firstly, the cobalt oxide were highly dispersed in silica support due to the structure of POSS compound IV. Compound IV possesses 16 carboxylic acid



groups coupling with cobalt in eight corners on the periphery. It is well known that better dispersion of cobalt species results in higher catalytic activity. Secondly, the POSS structure can prevent cobalt oxide from sintering during the thermal treatment. Finally, the morphology of POSS supported cobalt oxide after calcination would be more uniform with narrower size distribution. The above advantages made the catalysts much more active compared to the general silica supported cobalt oxide catalyst.

**Synthesis of supported cobalt oxide nanocrystals.** The supported cobalt oxide were generated by the calcination of the as-prepared pink cobalt nanospheres under 100 cc/min dry air (medical grade, Airgas) at 150°C, 550°C, 650°C respectively, for 6 hours with a 5°C/min temperature ramp. The as-synthesized catalysts were labelled as Co<sub>3</sub>O<sub>4</sub>-150, Co<sub>3</sub>O<sub>4</sub>-550, Co<sub>3</sub>O<sub>4</sub>-650, respectively.

### Characterization

<sup>1</sup>H, <sup>13</sup>C and <sup>29</sup>Si nuclear magnetic resonance (NMR) spectra were recorded with a Varian INOVA 400 spectrometer, operated at 400 MHz for <sup>1</sup>H, 100 MHz for <sup>13</sup>C, and 79 MHz for <sup>29</sup>Si. NMR spectra of the moisture sensitive compound were recorded in sealed J. Young NMR tubes. The <sup>1</sup>H and <sup>13</sup>C NMR chemical shifts, reported relative to SiMe<sub>4</sub>, were determined by reference to the residual <sup>1</sup>H solvent resonances. <sup>29</sup>Si NMR chemical shifts were referenced to TMS at 0.0 ppm. The chemical shifts reported are in ppm and coupling constants in Hz. Scanning electron microscopy (SEM) images were collected by a FE-SEM, Hitachi S-4800-II. High angle annular dark field (HAADF) scanning transmission electron microscope (STEM) images were obtained using a JEOL 2100-F transmission electron microscope (TEM) with a field emission gun at 200 kV, which has a spatial resolution of 0.2 nm. Particle size analyses were performed using the program Image J. X-ray diffraction (XRD) patterns were collected by Scintag XDS2000, Cu-K $\alpha$  radiation ( $\lambda=1.5418$  Å) at 40 kV, scan range  $2\theta = 5^\circ-90^\circ$ , and step rate = 0.05°/s. The size of the cobalt oxide nanoparticles was calculated using the Debye-Scherrer formula from the full width at half maximum (FWHM) of the (3 1 1) diffraction peak. X-ray photoelectron spectroscopy (XPS) spectra were collected by Omicron ESCA Probe equipped with an electron flood gun, Al-K $\alpha$  radiation at 1486.6 eV). The XPS binding energies were calibrated with respect to adventitious carbon (C1s). Fourier transform infrared (FT-IR) spectra were taken on Thermo Nicolet NEXUS 670 Fourier Transform infrared spectroscopy. The Brunauer-Emmett-Teller (BET) surface area was determined from equilibrium and saturation pressures measured by a Micromeritics ASAP 2010.

### Catalytic test with as-synthesized catalysts

Catalytic reactions were carried out according to the following procedure. 1.04 g of styrene (10 mmol), 30 mg of supported cobalt oxide catalysts were mixed in 20 ml of acetonitrile in a 50ml sealed glass reactor. Then the mixture was heated to 60 °C under constant vigorous stirring in an oil bath. After that 3.4 mL of H<sub>2</sub>O<sub>2</sub> (30 mmol) solution (30 wt. % in H<sub>2</sub>O, Sigma Aldrich) was added to the reactor at one time. Then the mixture was stirred for another 8 hours under atmospheric pressure. The products were analysed by a gas chromatograph (Varian star 3400 CX) with DB-624column (Agilent, 30m, 0.25mm, 1.40 $\mu$ m) and a flame ionization detector.

## Results and discussion

### Formation of pink cobalt nanospheres

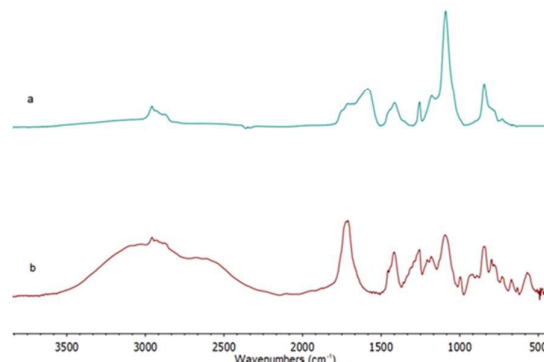


Fig. 2 FT-IR spectra of (a) cobalt nanospheres and (b) Compound IV.

The pink cobalt nanospheres was synthesized via the reaction of Co<sub>2</sub>(CO)<sub>8</sub> with Compound IV in the mixture of toluene and THF as previously described. Compound IV possesses 16 carboxylic acid groups on the periphery. The carboxylic acid can be used to anchor cobalt cations in the interior of several carboxylic acid groups and CO was released during this reaction. This reaction resulted in a pink precipitate of uniform, spherical globules. The FT-IR spectrum of compound IV and prepared pink cobalt nanospheres were shown in Fig. 2. The FT-IR spectrum (Fig. 2b) of the compound IV shows an intense band at 1715cm<sup>-1</sup> (-C=O in the -COOH group), while the cobalt nanospheres after the reaction have a strong band at 1583 cm<sup>-1</sup>, indicating the formation of -COO- group. The remained, relatively weak band at 1715 cm<sup>-1</sup> suggests that there are still some carboxylic acid groups, possibly on the surfaces of the nanospheres. XRD spectra (Fig. S4) show two diffraction peaks at  $2\theta = 12.4^\circ$  and  $25.6^\circ$ , which are the feature peaks of spherosilicate carboxylate with POSS network structure. We replaced Co<sub>2</sub>(CO)<sub>8</sub> with Fe and Pd precursor following the similar procedure, similar XRD spectra were observed in the case of Fe and Pd. XPS spectra of the precipitate were recorded and the Co 2p spectra for the catalysts are shown in Figure 3a. The binding energy of Co 2p<sub>3/2</sub> is approximately 782.5 eV, indicating the formation of Co(II)<sup>25, 26</sup>. Apparently, Co<sub>2</sub>(CO)<sub>8</sub> was oxidized when reacting with carboxylic acids, leading to the formation of spherosilicate carboxylate- Co(II) cross-linking network. Based on the ICP data, the Co content is determined to be 10.01 wt%, suggesting that 4 Co cations are coordinated with 16 carboxyl groups.

### Particle size and morphology determination of supported cobalt oxide nanoparticles

**Powder X-ray diffraction (PXRD).** Fig. 3 shows the PXRD patterns of the supported cobalt oxide catalysts after calcination at different temperature, with a standard spectra of Co<sub>3</sub>O<sub>4</sub> as a reference. We imported all standards of cobalt oxide, like CoO, Co<sub>2</sub>O<sub>3</sub>, Co<sub>3</sub>O<sub>4</sub>, Co(OH)<sub>3</sub>, etc. However, the diffraction peaks of the product showed the fitness to characteristic peaks of Co<sub>3</sub>O<sub>4</sub>. The standard Co<sub>3</sub>O<sub>4</sub> shows diffraction peaks at  $2\theta = 19.0^\circ, 31.2^\circ, 36.8^\circ, 38.5^\circ, 44.8^\circ, 55.6^\circ, 59.3^\circ, 65.2^\circ, 68.6^\circ, 74.1^\circ$  and  $77.3^\circ$ , indicated the crystallized

spinel  $\text{Co}_3\text{O}_4$  with space group  $\text{Fd}3\text{m}$ : crystallochemical formula  $\text{Co}^{2+}\text{Co}_2^{3+}\text{O}_4$ , where  $\text{Co}^{3+}$  occurs in the octahedral position and  $\text{Co}^{2+}$

spectra further suggests that the product mainly composed of  $\text{Co}_3\text{O}_4$ .<sup>30</sup>

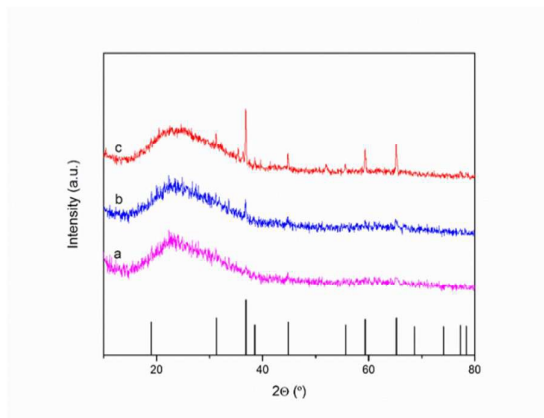


**Fig. 3** XRD spectra of (a)  $\text{Co}_3\text{O}_4$ -150, (b)  $\text{Co}_3\text{O}_4$ -550, (c)  $\text{Co}_3\text{O}_4$ -650 and standard spectra of  $\text{Co}_3\text{O}_4$ .

occurs in the tetrahedral position<sup>27, 28</sup>. As expected, spherosilicate structure (POSS) shows a broad peak at  $15^\circ < 2\theta < 30^\circ$ , corresponding to the amorphous structure of the Si-O-Si clustering, which served as the support of cobalt oxide. Catalyst  $\text{Co}_3\text{O}_4$ -150 (Fig. 3a) did not display any sharp diffraction pattern but a very broad and slight peaks attributed to cobalt oxide. The signals were very weak, likely due to the thermal decomposition just started and only very small amount of cobalt oxide products formed. The catalyst  $\text{Co}_3\text{O}_4$ -550 (Fig. 3b) showed very broad diffraction peaks at  $2\theta = 36.6^\circ$ ,  $44.7^\circ$ ,  $65.1^\circ$ , indicated the formation of nanocrystalline product. The average particle size, calculated by X-ray line broadening through the Scherrer equation, was 11 nm which was consistent with the TEM images. The distinct peaks of catalyst  $\text{Co}_3\text{O}_4$ -650 indicate the formation of large cobalt oxide particles with high crystallinity, and the average diameter of  $\text{Co}_3\text{O}_4$  is calculated to be 70 nm based on Scherrer equation (Fig. 3c). When comparing  $\text{Co}_3\text{O}_4$ -650 and  $\text{Co}_3\text{O}_4$ -550, the former shows narrower peaks with stronger intensity, which is the evidence for the formation of larger  $\text{Co}_3\text{O}_4$  crystals.

**XPS spectra.** XPS measurements were carried out to obtain further insight into the oxidation state of cobalt in the supported catalysts. As we discussed previous, the XPS spectrum of the pink cobalt nanospheres (Fig. 4a) shows the peak of  $\text{Co } 2p_{3/2}$  located at  $\sim 782.5$  eV indicating the formation of  $\text{Co(II)}$ <sup>26</sup>. Commercial  $\text{Co}_3\text{O}_4$  (Figure 4e) showed the  $\text{Co } 2p_{3/2}$  peak located at  $\sim 780.2$  eV and the  $\text{Co } 2p_{1/2}$  peak located at  $\sim 795$  eV. For the three catalysts after calcination, the  $\text{Co } 2p$  peak shifted a little bit to the lower binding energy with the temperature increase. While the peak located very close to commercial  $\text{Co}_3\text{O}_4$  (Figure 4b-d), indicating that the cobalt oxide supported on silica likely fits the stoichiometry of  $\text{Co}_3\text{O}_4$ . That was in good accordance with XRD data. The  $\text{Co } 2p$  XPS spectra showed two major peaks with BE values at 795.6 and 780.2 eV, corresponding to the  $\text{Co } 2p_{1/2}$  and  $\text{Co } 2p_{3/2}$  spin-orbit peaks, respectively, of the  $\text{Co}_3\text{O}_4$  phase.<sup>29</sup> The  $\text{Co } 2p_{1/2}$ - $\text{Co } 2p_{3/2}$  energy separation was approximately 15.4 eV. Lack of prominent shake-up satellite peaks in the  $\text{Co } 2p$

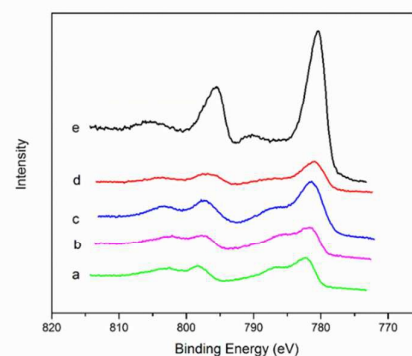


**Fig. 4** Co 2p XPS spectra of (a) cobalt nanospheres before calcination, (b)  $\text{Co}_3\text{O}_4$ -150, (c)  $\text{Co}_3\text{O}_4$ -550, (d)  $\text{Co}_3\text{O}_4$ -650 and (e) commercial micrometer  $\text{Co}_3\text{O}_4$ .

The XPS spectra of Si 2p are shown in Fig. S5. The cobalt nanospheres before calcination (Fig. S5a) shows two peaks at  $\sim 103.5$  eV and  $\sim 101.2$  eV, indicating that two types of Si-O bond exist in the compound. It can be inferred that one can be assigned to Si-O-Si in POSS structure and the other to O-Si- $\text{CH}_x$ . After calcination, most of the hydrocarbons were burnt down and Si-O bond can form clustering Si-O-Si bond, which is pretty similar to the Si-O-Si bond in POSS structure. Therefore, the peak of Si 2p became sharper and the shoulder becomes smaller as the calcination temperature increased.

**SEM and (HAADF) STEM images.** Fig. 5a-c showed the SEM images of samples obtained before calcination and after calcination at 150 °C and 550 °C, respectively. Silica-supported cobalt nanospheres with monodisperse size dispersion were achieved using our synthetic approach (Fig. 5a). These nanospheres had a mean diameter of 200 nm. After calcination at 150 °C (Fig. 5b, 5d), the morphology was maintained upon formation of the  $\text{Co}_x\text{O}_y$  clusters since the temperature was not high enough for the thermal decomposition or cobalt oxide crystallization. Probably very small amount cobalt oxide nanocrystalline already formed.

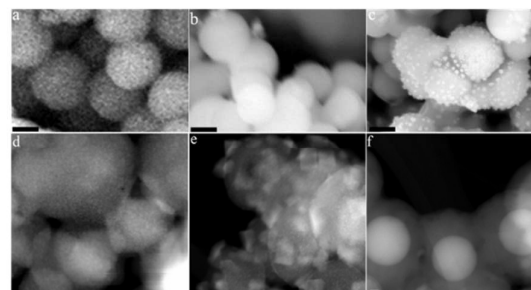


**Fig. 5** SEM images of (a) cobalt nanospheres before calcination, (b)  $\text{Co}_3\text{O}_4$ -150, (c)  $\text{Co}_3\text{O}_4$ -550. STEM images (d)  $\text{Co}_3\text{O}_4$ -150, (e)  $\text{Co}_3\text{O}_4$ -550, (f)  $\text{Co}_3\text{O}_4$ -650. Scale bars are 100 nm in (a-c) and 15 nm in (d-f).

## Journal Name

## ARTICLE

**Table 1** Selective oxidation of styrene on supported cobalt oxide catalysts.

Catalyst	[Co] <sup>a</sup> (wt %)	Particle size calculated from XRD		Conv. (%)	Selectivity(%)			TOF <sup>b</sup>	BET (m <sup>2</sup> g <sup>-1</sup> )
		Before reaction	After reaction		Styrene epoxide	Benzaldehyde	Other product		
Co <sub>3</sub> O <sub>4</sub> -150	9.1	N/A <sup>c</sup>	N/A <sup>c</sup>	12	80	15	5	3.3	15
Co <sub>3</sub> O <sub>4</sub> -550	8.4	11	12	97	91	5	4	28.3	46
Co <sub>3</sub> O <sub>4</sub> -650	8.1	70	73	27	96	2	2	8.2	42

Reaction conditions: Catalyst weight = 30 mg. <sup>a</sup>Determined by ICP-AES. <sup>b</sup>mol(C<sub>8</sub>H<sub>8</sub>converted)/mol(Co)<sup>-1</sup>h<sup>-1</sup>. <sup>c</sup>The peak is too weak to do the calculation from X-ray line broadening.

With the calcination temperature increased to 550°C, the SEM images (Fig. 5c) showed the integrity of the spinel nanostructure. Fig. 5e showed a typical STEM image of the nanostructure with high crystallinity. The chemical compositions of the as-prepared nanocrystals have been investigated by EDS. Results from EDS elemental analysis for the nanocrystals on the surface of Co<sub>3</sub>O<sub>4</sub>-550 sample showed that the nanocrystals contain Co and O. The atomic ratio of Co to O is 42:58, which matched the stoichiometry of Co<sub>3</sub>O<sub>4</sub> quite well. Basically based on the elemental mapping images (Fig. S6a) we noticed that Co<sub>3</sub>O<sub>4</sub> nanocrystals were developed and supported on silica which was consistent with the XRD results. Herein, the corners and edges of Co<sub>3</sub>O<sub>4</sub> nanocrystals can be clearly observed.

As the calcination temperature further increased to 650°C, cobalt oxides like egg yolk were formed exclusively inside the supported silica (Fig. 5f, Fig. S6b). The yolk shaped crystals consist of parallel bundles of nanocrystals whose structure is confined by the supported silica channels. The crystals were linked by short bridges, formed by Co<sub>3</sub>O<sub>4</sub> growth in the micropores interconnecting the microscale channels. We estimated that the yolkshaped cobalt oxide may be formed through a redissolving and redepositing process under thermal conditions<sup>31, 32</sup>.

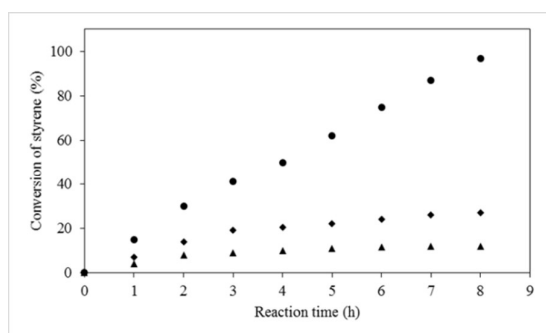


**Fig. 6** The conversion of styrene as a function of reaction time (▲) Co<sub>3</sub>O<sub>4</sub>-150, (●) Co<sub>3</sub>O<sub>4</sub>-550, (◆) Co<sub>3</sub>O<sub>4</sub>-650.

Our studies indicate that the morphology and size of final products strongly depend on calcination conditions such as temperature and time. Study on the effects of calcination time shows that spinel cobalt oxide nanocrystals gradually form with increasing calcination time. Six hours are enough for the crystallization process. Generally, the size and the morphology of the cobalt oxide nanostructure could be manipulated by changing calcination temperature and hydrothermal time.

**Catalytic activity of supported cobalt oxide nanocrystals with different morphologies.** The as-synthesized cobalt oxide nanocrystals were used as the catalyst for the oxidation reaction of styrene, in which hydrogen peroxide was used as the oxidant. The performance of each catalyst is summarized in Table 1. Under the reaction conditions, all catalysts gave quantitative conversions after 8 h of reaction, the two main products being styrene oxide and benzaldehyde in all cases. The cobalt content in all three catalysts are around 8-9 wt% more or less based on the ICP-AES results. However, they performed totally different catalytic activity under the same reaction conditions. Typically Co<sub>3</sub>O<sub>4</sub>-550 showed substantially higher activity than that of Co<sub>3</sub>O<sub>4</sub>-150 and Co<sub>3</sub>O<sub>4</sub>-650. Besides, Co<sub>3</sub>O<sub>4</sub>-550 showed relatively high selectivity to styrene epoxide as high as 91%, almost close to the selectivity over Co<sub>3</sub>O<sub>4</sub>-650 sample (96%). Taken together, Co<sub>3</sub>O<sub>4</sub>-550 was the best catalyst due to the high activity and high selectivity for styrene oxidation. Co<sub>3</sub>O<sub>4</sub>-550 manifested so excellent catalytic properties, on one hand, due to the high crystallinity of Co<sub>3</sub>O<sub>4</sub> formed on the support and the nanocrystals size and the morphology are more active for styrene oxidation. The particle size calculated from XRD line broadening measurements were listed in Table 1, column 3 and 4. The particle size before and after the catalytic test remained about the same within uncertainties. It was found that the turnover frequency increases from 8.2 to 28.3 with decreasing cobalt oxide particle size, which was attributed to the increasing fraction of edge and corner surface sites with decreasing size. Therefore, it was concluded that the smaller Co<sub>3</sub>O<sub>4</sub> particles perform better in catalysis of styrene oxidation. On the other hand, the BET surface area of Co<sub>3</sub>O<sub>4</sub>-550 after thermal treatment (Table 1, last column) is larger compared to the other two samples, which can absorb more reactants and offer

more active sites in the reaction. However, the selectivity to epoxide is a little bit lower than  $\text{Co}_3\text{O}_4$ -650.  $\text{Co}_3\text{O}_4$ -650 with the larger cobalt oxide size nanoparticles showed better selectivity to styrene oxide, which was as high as 96%. We conjectured that the selectivity of the reaction is dependent on the silica framework used for the stabilization of the cobalt oxide NPs, with the 3D channel framework of the support providing higher selectivity. The reactants and products can only be selected to pass the channel of the silica support. For  $\text{Co}_3\text{O}_4$ -550,  $\text{Co}_3\text{O}_4$  nanocrystals outside of the silica support could lower the selectivity to some degree.

We have further investigated the reaction kinetics by monitoring the time-dependent conversion of styrene in the system (Fig. 6). When  $\text{Co}_3\text{O}_4$ -550 was used as the catalyst, the conversion of styrene increases roughly linearly with reaction time, reaching 97% within 8h. However, for  $\text{Co}_3\text{O}_4$ -150 catalyst, the conversion of styrene slightly increased with reaction time and reached quasi-equilibrium after 4h. Totally the conversion after 8h was only 12%. For  $\text{Co}_3\text{O}_4$ -650, a similar trend in activity was observed, while the conversion was much higher than  $\text{Co}_3\text{O}_4$ -150 catalyst. We conjectured that in the first 4 hours the  $\text{H}_2\text{O}_2$  was quite reactive and can readily be activated even with larger cobalt oxide catalysts. While after several hours, the reactants and products reached equilibrium on cobalt oxide surface which might block the exposed active sites. Besides, as presented distinctly in Fig. S7, the increase of styrene concentration from 0.5mmol to 2.5 mmol caused almost a linear reduction of styrene conversion from 97 to 71% at 333 K. However, the increase of styrene concentration had small influence on the selectivity to epoxide, which exhibited a small decrease from 93% to 87%. We concluded that the contact of hydrogen oxide to active site of  $\text{Co}_3\text{O}_4$ -550 might be a rate determining step at this reaction. All in all, different morphology of the supported cobalt oxide nanocrystals performed differently in styrene oxidation reaction. By controlling the synthetic parameter, we can prepare the active catalyst with appropriate morphology in catalytic reaction.

For the development of cost-effective, green, and benign industrial processes, catalyst stability and recycling are very important. In metal-containing heterogeneous catalysts, the leaching of the active metal from the supported materials is often a

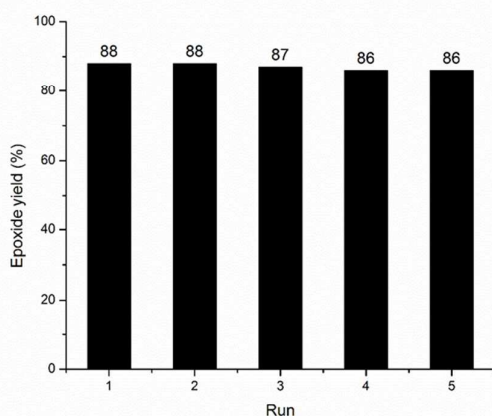


**Fig. 7** Recycling of the active  $\text{Co}_3\text{O}_4$ -550 catalyst for the epoxidation of styrene. Run 1 is with fresh catalyst.

problem. Such leaching processes result in diminished reactivity and selectivity in catalytic processes. When studying the recycling of active catalyst  $\text{Co}_3\text{O}_4$ -150 system, the solution after the reaction was cooled down and 100 mL  $\text{CH}_3\text{CN}$  was added. Then the solid was filtered and dried in the oven for the next run under the same conditions. Fig. 7 showed the epoxide yield after 5 recycling experiments with the use of  $\text{Co}_3\text{O}_4$ -550. The catalyst was still active and a similar conversion was observed like the fresh use. In brief,  $\text{Co}_3\text{O}_4$ -550 was a pretty proper catalyst for styrene oxidation with high conversion and high selectivity and can be used repeatedly.

## Conclusions

Metal oxide nanoparticles with controlled morphology are crucial due to the strong correlation between these parameters and their catalytic properties. In this paper, we demonstrated a practical, convenient and facile method to prepare supported cobalt oxide nanoparticles with controlled size and morphology. The synthesis was mediated by thermal treatment temperature and permitted controlled variation of metal oxide particle size and morphology at nanometer scale. In the present work three samples  $\text{Co}_3\text{O}_4$ -150,  $\text{Co}_3\text{O}_4$ -550 and  $\text{Co}_3\text{O}_4$ -650 were successfully synthesized and as synthesized samples with different morphologies exhibited totally different properties for the oxidation of styrene. Monitor the synthesis with SEM, TEM, XRD, EDS and XPS at different calcination stages and optimize the catalyst for the target reaction.  $\text{Co}_3\text{O}_4$ -550 resulted in extraordinary activity with relatively high selectivity to epoxide. Thus, the results reported here indicated that nanocrystalline cobalt oxide supported on silica by this method are very promising catalysts for the selective oxidation of olefins. We concluded that different morphology of metal oxide nanoparticles performed differently in catalytic reaction. By controlling the synthetic parameter, we can prepare the active catalyst with appropriate morphology in catalytic reaction. Moreover, in developing large-scale processes, heterogeneous catalytic systems have many advantages including easy removal of catalysts from reaction mixtures and recycling of catalysts. In conclusion, the method is very versatile because the carboxylic acid ligand can easily couple to metal carbonyl and many other commercially available metal precursors, in addition to Co, such as Pd, Fe, Ni, etc (to be reported later). Thus, it could have many potential applications when such particles are called for, such as in sensors and catalysis.

## Acknowledgements

This research was supported by the Specialized Research Fund for NSF of China (51172184, 51572221); Specialized Research Fund for the Doctoral Program of the Ministry of Education (20116102110014). Z. W. and X. H. acknowledge the funding support from China Scholarship Council. This work made use of the SEM, TEM and NMR in the EPIC facility of NUANCE Center and IMSERC facility at Northwestern University.

## Notes and references

‡ Z. Wang and X. Hou contributed equally in this paper.

- 1 C. N. R. Rao and A. K. Cheetham, *Journal of Materials Chemistry*, 2001, 11, 2887-2894.
- 2 P. Poizot, S. Laruelle, S. Grugeon, L. Dupont and J. M. Tarascon, *Nature*, 2000, 407, 496-499.
- 3 C. N. P. Dafonseca, M. A. Depaoli and A. Gorenstein, *Advanced Materials*, 1991, 3, 553-554.
- 4 S. Takada, M. Fujii, S. Kohiki, T. Babasaki, H. Deguchi, M. Mitome and M. Oku, *Nano letters*, 2001, 1, 379-382.
- 5 K. Takada, H. Sakurai, E. Takayama-Muromachi, F. Izumi, R. A. Dilanian and T. Sasaki, *Nature*, 2003, 422, 53-55.
- 6 C. Cantalini, M. Post, D. Buso, A. Guglielmi and A. Martucci, *Sensors and Actuators B-Chemical*, 2005, 108, 184-192.
- 7 M. Ando, T. Kobayashi, S. Iijima and M. Haruta, *Journal of Materials Chemistry*, 1997, 7, 1779-1783.
- 8 B. Solsona, T. E. Davies, T. Garcia, I. Vazquez, A. Dejoz and S. H. Taylor, *Appl Catal B-Environ*, 2008, 84, 176-184.
- 9 T. E. Davies, T. Garcia, B. Solsona and S. H. Taylor, *Chemical Communications*, 2006, 32, 3417-3419.
- 10 G. Laugel, J. Arichi, H. Guerba, M. Moliere, A. Kiennemann, F. Garin and B. Louis, *Catalysis letters*, 2008, 125, 14-21.
- 11 I. Yuranov, L. Kiwi-Minsker and A. Renken, *Appl Catal B-Environ*, 2003, 43, 217-227.
- 12 L. Zhou, J. Xu, H. Miao, F. Wang and X. Li, *Applied Catalysis a-General*, 2005, 292, 223-228.
- 13 I. Lopes, A. Davidson and C. Thomas, *Catalysis Communications*, 2007, 8, 2105-2109.
- 14 Y. Li, B. Tan and Y. Wu, *Journal of the American Chemical Society*, 2006, 128, 14258-14259.
- 15 T. Li, S. Yang, L. Huang, B. Gu and Y. Du, *Nanotechnology*, 2004, 15, 1479-1482.
- 16 X. H. Liu, G. Z. Qiu and X. G. Li, *Nanotechnology*, 2005, 16, 3035-3040.
- 17 X. Shi, S. Han, R. J. Sanedrin, C. Galvez, D. G. Ho, B. Hernandez, F. Zhou and M. Selke, *Nano letters*, 2002, 2, 289-293.
- 18 X. Shi, S. Han, R. J. Sanedrin, F. Zhou and M. Selke, *chemistry of Materials*, 2002, 14, 1897-1902.
- 19 S. Ladas, *Surface Science*, 1986, 175, L681-L686.
- 20 R. B. Greegor and F. W. Lytle, *Journal of Catalysis*, 1980, 63, 476-486.
- 21 X. Xie and W. Shen, *Nanoscale*, 2009, 1, 50-60.
- 22 M. E. Grass, Y. Zhang, D. R. Butcher, J. Y. Park, Y. Li, H. Bluhm, K. M. Bratlie, T. Zhang and G. A. Somorjai, *Angewandte Chemie-International Edition*, 2008, 47, 8893-8896.
- 23 G. A. Somorjai and N. Materer, *Topics in Catalysis*, 1994, 1, 215-231.
- 24 Z. Shen, J. Kim, J. Shen, C. M. Downing, S. Lee, H. H. Kung and M. C. Kung, *Chemical Communications*, 2013, 49, 3357-3359.
- 25 B. W. Lee, A. Ignatiev, J. A. Taylor and J. W. Rabalais, *Solid State Communications*, 1980, 33, 1205-1208.
- 26 C. Wagner and G. Muilenberg, *Handbook of X-ray photoelectron spectroscopy*, Perkin-Elmer, 1979.
- 27 G. Laugel, J. Arichi, M. Moliere, A. Kiennemann, F. Garin and B. Louis, *Catalysis today*, 2008, 138, 38-42.
- 28 J. Taghavimoghaddam, G. P. Knowles and A. L. Chaffee, *Journal of Molecular Catalysis a-Chemical*, 2012, 358, 79-88.
- 29 C. V. Schenck, J. G. Dillard and J. W. Murray, *Journal of Colloid and Interface Science*, 1983, 95, 398-409.
- 30 M. A. Langell, M. D. Anderson, G. A. Carson, L. Peng and S. Smith, *Physical Review B*, 1999, 59, 4791-4798.
- 31 W. Wang, C. Xu, G. Wang, Y. Liu and C. Zheng, *Advanced Materials*, 2002, 14, 837-840.
- 32 P. W. Voorhees, *Annual Review of Materials Science*, 1992, 22, 197-215.

## Supported Cobalt Oxide Nanocrystals: Morphology Control and Catalytic Performance For Styrene Oxidation

Zhen Wang,<sup>‡a</sup> Xianliang Hou,<sup>‡a</sup> Jingmei Shen<sup>b</sup> and  
Tiehu Li<sup>a\*</sup>

Supported cobalt oxide catalysts with controlled size and morphologies were facily synthesized and performed high activity for styrene oxidation.

